Draft version January 25, 2013
Preprint typeset using LaTeX style emulateapj v. 12/16/11

BRIGHT RAY-LIKE FEATURES IN THE AFTERMATH OF CMES: WHITE LIGHT VS UV SPECTRA

A. Ciaravella[1], D. F. Webb[2], S. Giordano[3] & J.C. Raymond[4]

Draft version January 25, 2013

ABSTRACT

Current sheets are important signatures of magnetic reconnection in the eruption of confined solar magnetic structures. Models of Coronal Mass Ejections (CMEs) involve formation of a current sheet connecting the ejected flux rope with the post eruption magnetic loops. Current sheets have been identified in white light images of CMEs as narrow rays trailing the outward moving CME core, and in ultraviolet spectra as narrow bright features emitting the [Fe XVIII] line. In this work samples of rays detected in white light images or in ultraviolet spectra have been analyzed. Temperatures, widths, and line intensities of the rays have been measured, and their correlation to the CME properties has been studied. The samples show a wide range of temperatures with hot, coronal and cool rays. In some cases, the UV spectra support the identification of rays as current sheets, but they show that some white light rays are cool material from the CME core. In many cases, both hot and cool material are present, but offset from each other along the UltraViolet Coronagraph Spectrometer (UVCS) slit. We find that about 18% of the white light rays show very hot gas consistent with the current sheet interpretation, while about 23% show cold gas that we attribute to cool prominence material draining back from the CME core. The remaining events have ordinary coronal temperatures, perhaps because they have relaxed back to a quiescent state.

Subject headings: Sun: coronal mass ejections (CMEs), UV radiation, Corona

1. INTRODUCTION

The loss of equilibrium in magnetic structures that disrupts coronal structures and ejects confined plasma into interplanetary space requires magnetic reconnection (Forbes 2000; Forbes et al. 2006; Low 2001). Dissipation of magnetic energy and topological reconfiguration of the magnetic field arise in strong current sheets, regions of large gradient in the tangential component caused by layers of antiparallel field lines. In the standard picture of solar eruptions, a current sheet connecting the flare loops to the CME core is where magnetic free energy is converted into thermal and bulk kinetic energies and into beams of energetic particles (Litvinenko 1996; Lin & Forbes 2000; Forbes et al. 2006). The reconnection must be rapid in order to explain the rapid rise times of flares, and current models stress kinetic effects (Priest & Forbes 2000), turbulence (Lazarian & Vishniac 1999; Emslie et al. 2004) or instabilities related to the tearing mode and the growth of magnetic islands (Loureiro 2007; Ji & Daughton 2011). To test these theories it is important to measure the physical parameters, such as temperatures, densities, velocities, turbulence and widths, of the current sheets.

Recent observational studies of current sheets include coronagraph observations in white light based on timing and morphology of rays that connect the eruption site to the apparent trailing edge of a CME flux rope (Webb et al. 1995, 2003) or based on coincidence of a bright feature with a current sheet identified from X-rays (Patsourakos & Vourlidas 2011). Vršnak et al. (2009) measured the properties of several such rays as functions of height and time. Song et al. (2012) analyzed the morphology of 11 white light rays that had plasma blobs flowing outwards sequentially along the ray. Four of their rays are also included in the sample studied in this paper.

In ultraviolet spectra, current sheets were identified as narrow regions of very hot plasma seen with UVCS between flare loops and CME cores (Ciaravella et al. 2002; Ko et al. 2003; Bemporad et al. 2006; Ciaravella and Raymond 2008; Schettino et al. 2010) or as hot gas with very large line widths above flare loops observed by the Solar Ultraviolet Measurements of Emitted Radiation (SUMER), (Innes et al. 2003; Wang et al. 2007). Narrow band EUV images also show hot gas in current sheets above the limb, notably the Transition Region and Coronal Explorer images of Innes et al. (2003) and the Solar Dynamics Observatory/Atmospheric Imaging Assembly (AIA) images of Reeves & Golub (2011) and Cheng et al. (2011). Current sheets have also been identified with X-ray emission above the flare loops (Sui & Holman 2003; Savage et al. 2010; Savage & McKenzie 2011).

In this paper we attempt to clarify the relationship between the white light and UV manifestations of current sheets, both to determine whether the identified features really are current sheets and to better constrain their physical properties. We approached the problem from two directions. First, we systematically searched for white light rays that meet criteria for identification as current sheets: The requirements of a 'disconnection event' morphology and location in wake of a CME led to 157 candidate current sheets from among many thousands of radial features in LASCO images. We then examined UVCS data to see whether they contained hot

[1] INAF-Osservatorio Astronomico di Palermo, P.za Parlamento 1, 90134 Palermo, Italy
[2] Institute for Scientific Research, Boston College, Newton, MA 02459, USA
[3] INAF-Osservatorio Astrofisico di Torino, via Osservatorio 20, 10025 Pino Torinese, Italy
[4] Harvard-Smithsonian Center for Astrophysics, 60 Garden Street, Cambridge, MA 02138, USA

gas. Second, we used the catalog of UVCS observations of CMEs in which current sheets or possible current sheets were indicated by narrow emission features in the [Fe XVIII] line. Again, this was a stringent criterion, as fewer than 20 such events have been found among the thousand CMEs in the UVCS CME catalog. We then examined the LASCO data for these events to see whether they corresponded to white light rays that met the current sheet criteria. The white light selected rays cover the periods 1996 April through 1998 December to sample solar minimum and the year 2001 to sample solar maximum. The UV selected rays were obtained from the period 1996 June through 2005 December.

The paper is organized as follows. In Section 2 the UV and White Light (WL) instruments used for the analysis are described. WL and UV selection of the rays is presented in Section 3. The analysis and results are in Section 4, and summary and conclusions are in Section 5.

2. UVCS AND LASCO OBSERVATIONS

The study we present in this paper is mainly based on the observations of two instruments aboard the Solar and Heliospheric Observatory, the Large Angle and Spectrometric Coronagraph Experiment (LASCO) and UVCS. LASCO C2 is a white light coronagraph, that continuously observes the solar corona from 2.3 to 6 $R_\odot$ with a cadence of about 20 min and a pixel size of 11.4″ (Brueckner et al. 1995). For those events in which the UVCS slit was located below the LASCO C2 occulter disk we also examined, whenever the data were available, the Mark-III or Mark-IV K-coronameter data from Mauna Loa Solar Observatory (MLSO). The MLSO coronagraphs are ground-based instruments that produce polarization brightness maps of the solar corona from 1.14 to 2.86 $R_\odot$ in the range 7000 - 9000 Å with a 3 min cadence. The typical observing period is from $\sim$ 17:00 to $\sim$ 02:00 UT each day. The data for some days show misalignment with LASCO images as large as 13°. In those cases, we adjusted the MLSO images by eye.

Unlike the WL coronagraph with its complete view of the solar corona, the UVCS spectrometer has a field of view defined by its narrow entrance slit 42′ long and up to 82″ wide. The slit can be placed at any polar angle and at heliocentric heights between 1.5 and 9 $R_\odot$. UVCS has two UV channels optimized to detect the O VI $\lambda\lambda$ 1032, 1037 doublet and HI Lyα lines, respectively, but it covers the wavelength range from 945 to 1270 Å in first order and from 473 to 635 Å in second order (see Kohl et al. 1995 for a detailed description). The OVI channel has a redundant path that allows detection of the HI Lyα line. The spatial pixels are 7″ and spectral pixels are 0.0993 Å (0.0915 Å for the redundant path) and 0.1437Å for the OVI and LYA channels, respectively. The radiometric calibration is discussed by Gardner et al. (2002). The second order calibration needed for the Si XII lines is uncertain, but we adopt factors of 0.14 and 0.09 lower efficiency for the $\lambda\lambda$ 521 and 499 lines, respectively. Due to telemetry limitations, UVCS can only observe the full wavelength range using low spatial and spectral resolution. A full range is usually obtained with a 10 by 2 pixel binning in the spatial and spectral ranges respectively. However, most of the UVCS observations are made with spatial resolution of 3 (21″) or 6 (42″) pixels and a reduced spectral range. Observations with high spectral and spatial resolution require masking the detector in order to select the wavelength range of interest with the desired spectral and spatial binning.

The UVCS daily observation schedule includes a synoptic program in which the corona is scanned between 1.5 and 3 $R_\odot$ at eight polar angles (PA) in about 10 hours, and special observations designed to observe specific objectives, such as streamers, coronal holes, CMEs etc. The synoptic program has changed over the years, with varying ranges of heliocentric heights observed, spatial and spectral resolutions and spectral range. Despite this, the spectra always included the O VI doublet, Si XII $\lambda\lambda$ 499 or 521, Lyα , Lyβ and C III Ł977. During most of 2001, the synoptic scans also included the high temperature line of [Fe XVIII] ($10^{6.8}$ K), but in 1996 through 1998 they did not. [Fe XVIII] is the key indicator of hot gas because it is only detected by UVCS above 1.5 $R_\odot$ in the wake of CMEs as bright spatially narrow features (Ciaravella et al. 2002; Ko et al. 2003; Bemporad et al. 2006; Ciaravella and Raymond 2008; Schettino et al. 2010) or hot blobs (Raymond et al. 2003).

Streamer studies, especially those devoted to elemental abundances, have a large wavelength coverage, often the full wavelength range. CME watch sequences are designed to have high cadence with typical exposure time of 120 or 200 s. The observations are at a constant height or switch between two heights. Typical observation heights are between 1.6 and 2.3 $R_\odot$, and they cover a broad ionization range from cool lines such as C III ($\sim 10^5$ K) to hot lines such as [Fe XVIII] .

3. RAY SELECTION

3.1. *White Light Sample*

The white light ray-like features we analyzed in this paper were selected from the LASCO C2 observations. A catalog of LASCO CMEs with trailing concave-outward structures and rays has been developed by Webb. A comprehensive paper on the results of analysis of the WL rays is in preparation (Webb 2012, in preparation).

Early studies found that about 20% of the CMEs showed concave-outward features in SMM and LASCO coronagraph data, and these were identified as magnetic disconnection events (Webb et al. 1995, 2003). Webb et al. (1995) examined SMM coronagraph data for bright rays in the wakes of CMEs that were coaxial with the CME and had outward-moving U- or V-shaped structures at the top. Recently, Howard et al. (2012) have presented beautiful examples of a few disconnection events seen in STEREO coronagraph data and tracked their evolution into the heliosphere. In Figure 1 the sequence of LASCO wavelet-processed images shows the CME on 2001 August 9 moving outwards and the bright ray behind it. During this event the pre-existing streamer has blown out and on August 10 at 02:06 UT the transient ray has started to form. This is an event wherein the ray becomes a new, reformed, streamer. The depletion of Si XII emission, as well as Lyα and O VI in the region of the pre-CME streamer supports the LASCO movie interpretation of a ray-reforming streamer.

The selection criteria for the events in the WL catalog are essentially those described by Webb et al. (2003) and summarized above. Events were selected that had a

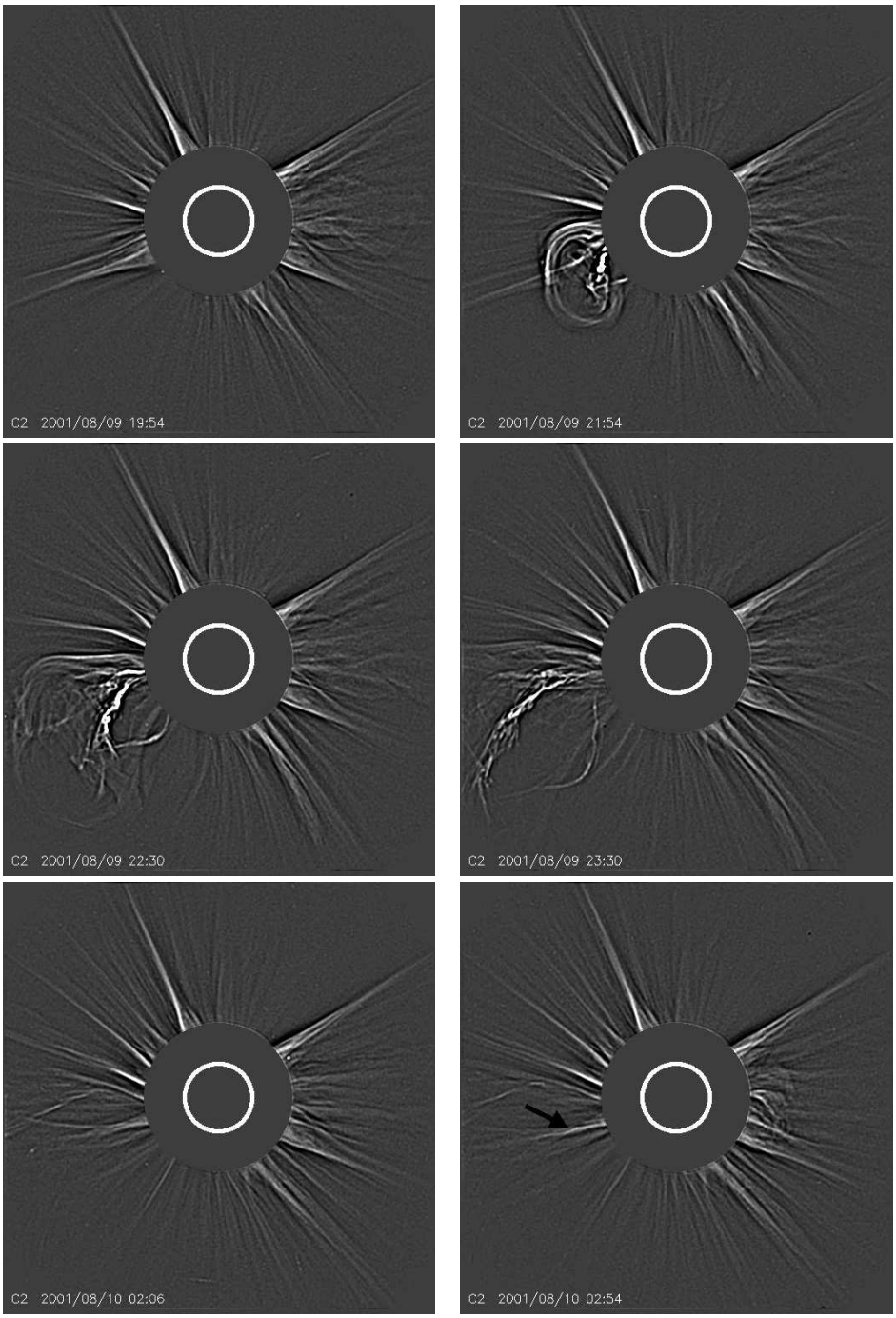

FIG. 1.— LASCO images of the CME on 2001 August 9. The images show the pre-CME corona (top left) at 19:54 UT and the CME evolution at 21:54, 22:30 and 23:30 UT. The bottom row shows the appearance of the ray at 02:06 UT and the clearly formed ray at 02:54 UT.

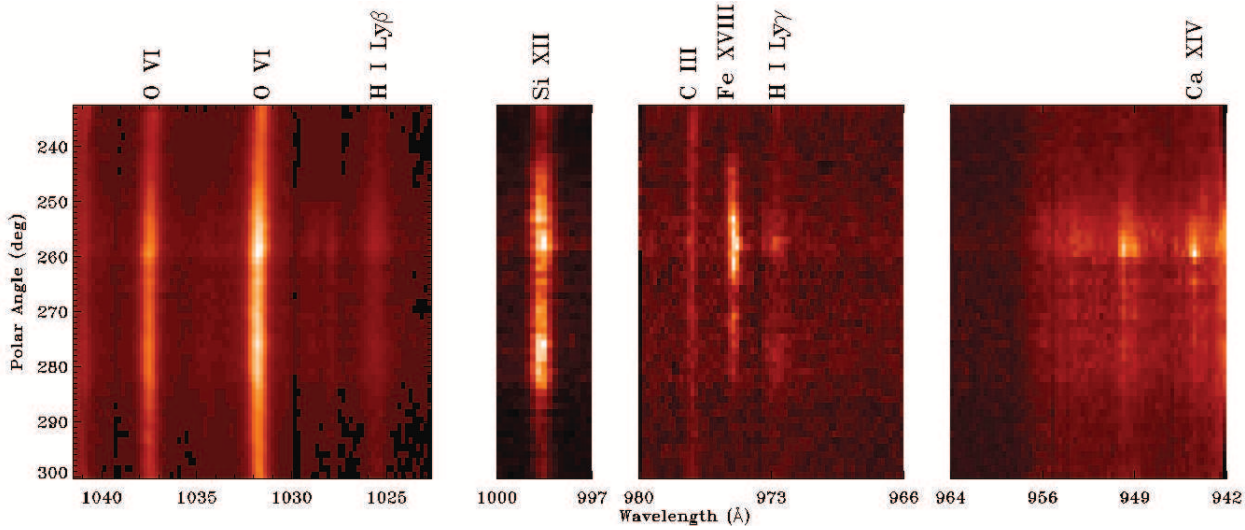

FIG. 2.— UVCS spectrum observed on 2003 June 2 after a CME. Some of the main lines are marked. The second order lines of Si XII Ł521 is the first line on the left of first panel, and Ł499 is in the second panel.

bright, narrow, linear ray following the concave-outward structure and coaxial within a few degrees with the CME volume. We required that such a ray appear within no more than about 12 hours following CME onset. Adequate data coverage was required during this period, ideally for at least a full day starting from just before CME onset to enable the identification of pre-existing structures, especially streamers, and whether a new streamer appeared in the wake of the CME and any ray. Indeed many of the WL rays form after streamer blowout and are associated with the subsequent reformation of the streamer (Webb et al. 2003). In our sample 29 events ($\sim 40\%$) are associated with streamer blowout, and in 7 cases the streamer forms afterward. For the events selected, we recorded the time when the ray appeared, its position angle and duration, along with the parameters of the CME. If Mauna Loa data for the appropriate time period were available, they were examined for the presence or absence of a corresponding ray. The ray-like features analyzed in this paper were selected from the LASCO ray catalog, mainly within the two temporal windows: from July 1996 to Dec 1998 during solar minimum, and 2001 for solar maximum. A total of 157 rays have been selected from LASCO images, of which 74 occur during the solar minimum period and 83 during the maximum. Once the white light rays were selected, UVCS archival data was examinaexaminedted for the existence of spectra at the appropriate position angle and time. There were cases in which UVCS did not observe any narrow bright feature corresponding to the WL ray. Of the 157 LASCO rays, 60 ($\sim 47\%$) had appropriate UVCS spectra showing bright features that matched the WL rays. Of these, 26 were found during the solar minimum period and 34 during solar maximum. Narrow bright features in the H I, O VI, Si XII and if possible [Fe XVIII] lines were searched for at the position angle of the white light feature. Some misalignment in position angle was tolerated because the features evolve in time and are not always radial, and most of the UVCS observations covered regions below the LASCO occulter height of 2.3 $R_\odot$. In general, if a UVCS feature was found, it was within about 3° of the LASCO position angle, but we include a few events with larger position angle differences. Most of the rays were detected during the daily synoptic scans, which unfortunately used a narrow spectral range and often did not include [Fe XVIII] line. We chose 2001 for this study because the synoptic sequence did include the [Fe XVIII] line.

3.2. *UVCS Sample*

In the wake of CMEs UVCS has observed several spatially narrow and bright features in the hot line of [Fe XVIII] that have been interpreted as signatures of the current sheet (CS) associated with CMEs (Ciaravella et al. 2002; Ko et al. 2003; Bemporad et al. 2006; Ciaravella and Raymond 2008). Figure 2 shows the spectrum of the CS associated with the CME on 2003 June 02 at 08:54 UT. The narrow bright feature in [Fe XVIII] appeared after the CME passed the UVCS field of view, and it was well aligned with the prominence core. This feature was also detected in the [Ca XIV] line in the fourth panel.

UVCS has observed more than a thousand CMEs and a catalog (Giordano et al. 2013), linked to the CDAW catalog of LASCO CMEs ($http://cdaw.gsfc.nasa.gov/CME\_list/$) was constructed by examining the UVCS data for each LASCO CME from the start of regular SOHO operations in 1996 through the end of 2005. For each white light CME, a special purpose computer code selected UVCS data at the position angle of the CME within 4 hours of the event. As part of the catalog, we determined whether there was an indication of a current sheet, usually by the presence of a narrow feature in [Fe XVIII] . For the present analysis, we examined the spectra of the 18 current sheets that showed clear features in [Fe XVIII] and compared them with LASCO data to determine whether a WL ray with current sheet morphology coincided with the UV feature. The sample includes the 6 events for which analysis of the current sheet has been previously published.

4. RAY ANALYSIS

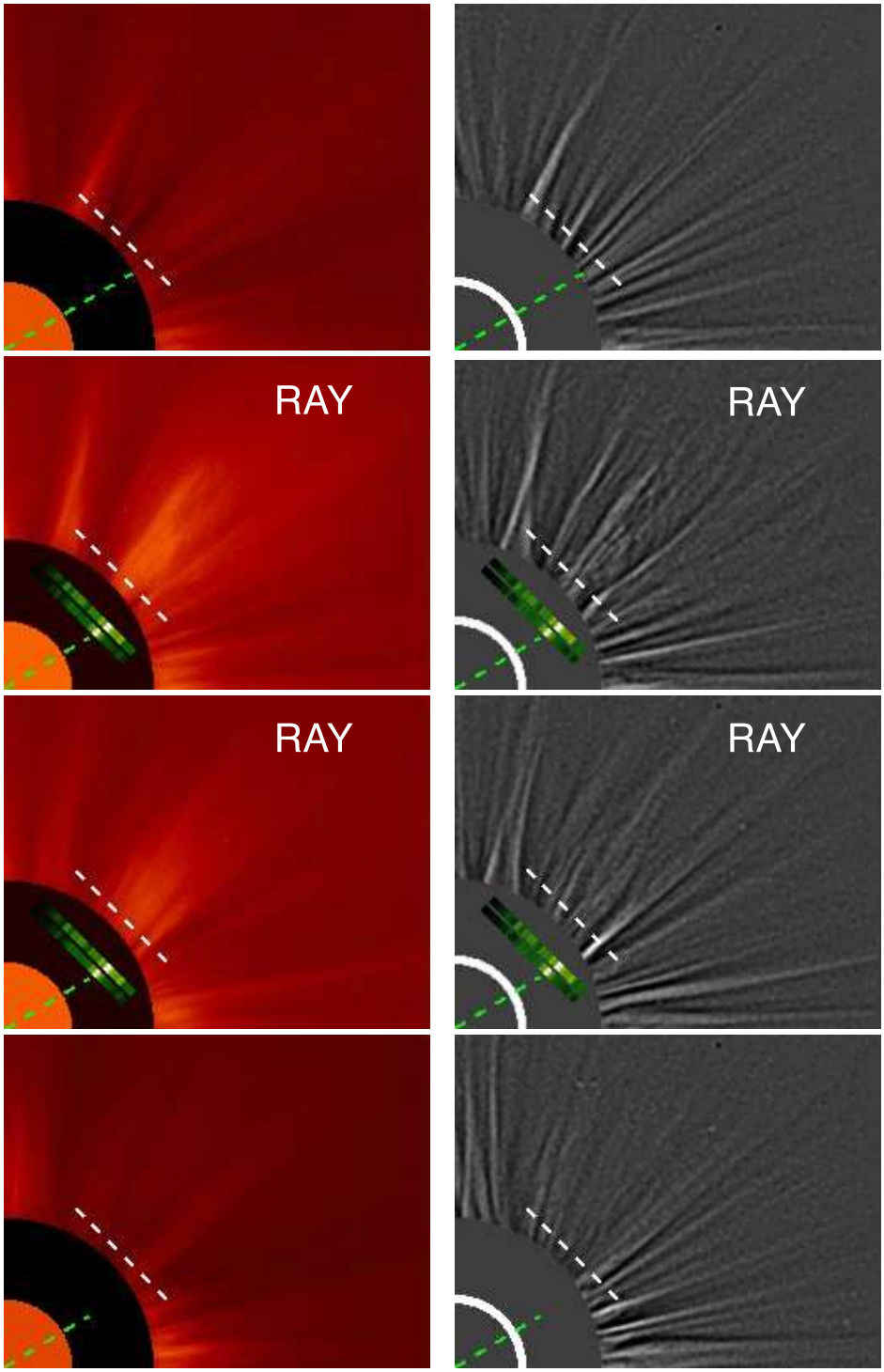

FIG. 3.— LASCO C2 images and wavelet-processed of the ray associated to the CME on 2000 September 23 at 21:30. The images show the pre-CME corona (top row) on 23rd at 20:26 UT, the ray in the wake of the CME (2nd and 3rd rows) on 24th at 01:27 and 10:26 UT and the post-ray corona (bottom row) on 24th on 23:50 UT. The green dashed line indicates the position of the WL ray. The images below the occulter are [Fe XVIII] along the UVCS slit taken on 23rd at 1.67 $R_\odot$ (from 22:19 to 22:28 UT) and at 1.53 $R_\odot$ (from 22:29 to 22:33 UT). The white dashed line at 2.4 $R_\odot$ marks the area where the LASCO data have been extracted to obtain the intensity distribution for Figure 4.

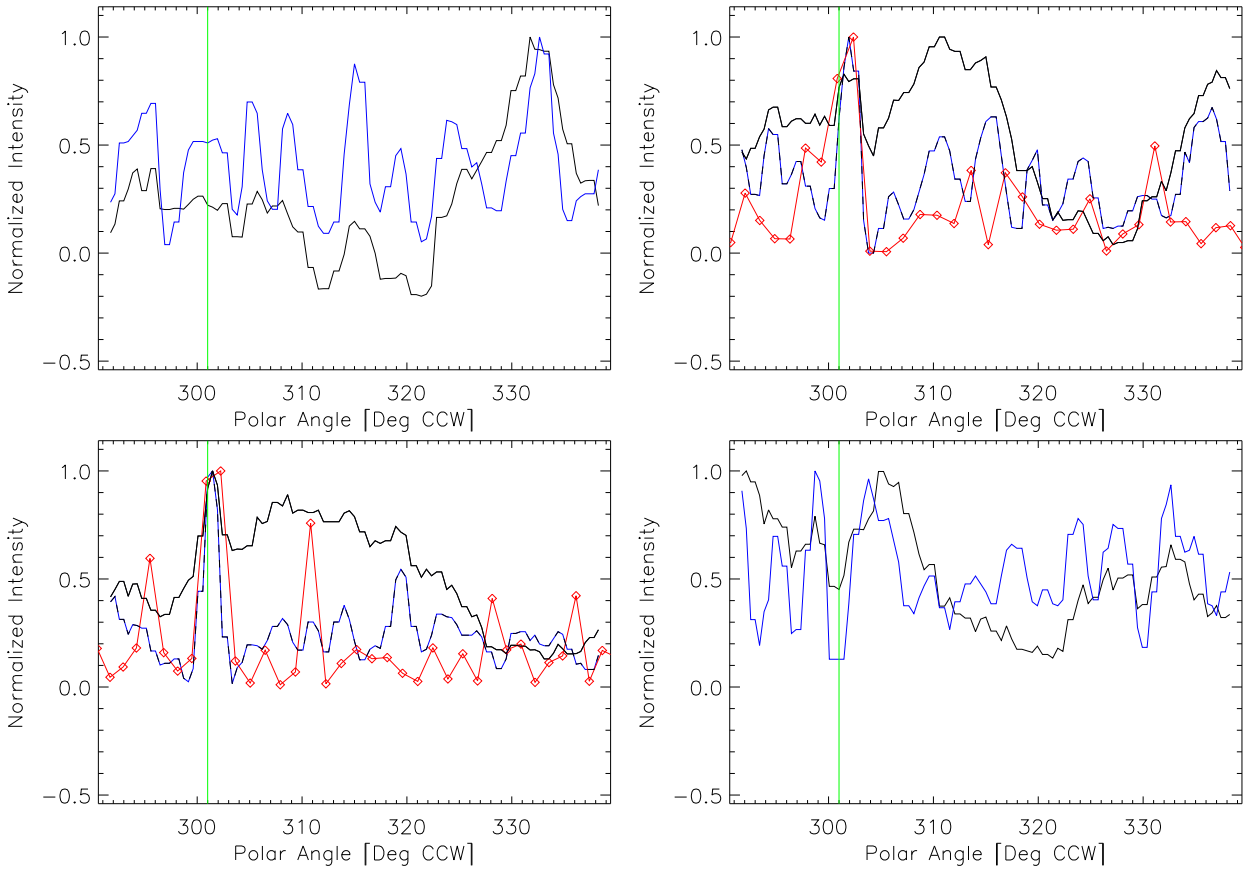

FIG. 4.— The four panels show the normalized intensities of LASCO C2 at 2.4 $R_\odot$ along the white segment in Figure 3. The green line marks the position of the ray in the WL images. Black and blue line correspond to LASCO background subtracted and wavelet-processed images respectively. The red line is the [Fe XVIII] line intensity along the UVCS slit at 1.67 (top right panel) and 1.53 $R_\odot$ (bottom left panel).

In our analysis we used LASCO WL background subtracted and wavelet-processed images. The background subtracted images have been obtained subtracting from LASCO raw images the related monthly minimum background and removing the spikes mainly due to the cosmic rays. The wavelet technique is particularly suitable for analysis of data containing discontinuities or sharp spikes and makes it possible to recover weak signals from noise. It uses mathematical functions to decompose data into different frequency components and then study each component with a resolution adapted to its scale. The wavelet-processed images from LASCO archive are based on a techniques developed by Stenborg & Gobelli (2003).

Before presenting our results we will describe the analysis method used for all the rays reported in this work by discussing in detail three events representative of hot, coronal and cool rays. We define hot as the rays that show [Fe XVIII] emission, coronal as those that are detected in Si XII and O VI , and cool rays as those that show emission only in the lines of O VI and/or Lyα . We note that O VI emission peaks at a temperature of about 0.3 MK, but that it persists up to about 2 MK due to dielectronic recombination of O VII. Lyα also peaks at low temperatures, but the combination of large hydrogen abundance and strong illumination by chromospheric Lyα photons combine to make it the strongest coronal UV line in spite of the 10^{-6} H I fraction. These lines seen in combination with coronal lines such as Si XII indicate a temperature similar to that of the corona. Bright emission in this lines without corresponding coronal emission lines indicates a temperature below 1 MK. This is often corroborated by very cool lines such as C III and by very narrow line widths.

Hot Ray (2000 September 23) - The WL images of the event have been analyzed before, during and after the CME in order to detect rays with the characteristics described in the previous paragraph. Figure 3 shows a sequence of LASCO and related wavelet-processed images for the event on 2000 September 23. ¿From the movies, images of the pre-CME corona (top row), of the ray in the wake of the CME (2nd and 3rd rows), and of the post-ray corona (bottom row) have been selected. The dashed green line in the images marks the position of the ray, the images below the occulter are the [Fe XVIII] images along UVCS slit obtained at 1.53 and 1.67 $R_\odot$. Both background subtracted and wavelet-processed images show clearly the formation of a new ray. The bright feature along the UVCS slit is well aligned with the WL ray. The pre-CME and post-ray coronal images in the [Fe XVIII] line do not show any sharp emission at the location of the ray. In Figure 4 we compare the normalized LASCO intensities along the white segment marked in Figure 3 with the normalized intensity of [Fe XVIII] (red line) along the UVCS slit at 1.53 $R_\odot$ (top right panel) and 1.67 $R_\odot$ (bottom left panel). The ray was not detected in the in Lyα , O VI or Si XII lines, see Table 1. [Fe XVIII] is the only line in which we detected a bright

peak at the the location of the WL ray, and this implies a temperature of $10^{6.8}$ K or higher. The black and blue lines correspond to the background subtracted and wavelet-processed LASCO images, respectively. While the LASCO intensities are extracted at 2.5 $R_\odot$ and the position of the UVCS entrance slit is below the LASCO occulter, the WL and UV ray are in good agreement. The UV ray at 1.53 $R_\odot$ is offset toward north by about 2°, probably because the ray is not exactly radial.

Coronal Ray (2001 May 12) - The LASCO C2 images of the events are in Figure 5 and show the pre-CME corona (top row), the ray in the wake of the CME (middle rows) and the post-ray corona (bottom row). The figure also shows the Si XII 499Å images along the UVCS slit. Before the CME and after the ray disappeared the UVCS slit was located below the occulter disk while during the lifetime of the ray, UVCS observed at 1.67 and 2.42 $R_\odot$. The ray is clearly visible in the background subtracted and wavelet-processed images. Si XII 499Å images show a narrow bright area at the position of the ray. Similar peaks are also observed in O VI and Lyα lines indicating typical coronal temperatures. This narrow bright area is not present in the UV spectra of the pre-CME and post-ray corona. As with the previous event the normalized intensities extracted along the white dashed lines in LASCO images or at the same location of the UVCS slit when it is located above the occulter and Si XII 499 Å are plotted in Figure 6. In the top right panel WL and Si XII intensities are at the same height, 2.42$R_\odot$, while in the bottom left panel Si XII intensity was detected at 1.67 $R_\odot$. Again the WL ray and UV bright narrow spots are well aligned.

Cool Ray (1998 April 23) - A cool ray is that associated with the CME on 1998 April 23 at 05:27 UT. The ray appeared in WL images at 10:55 UT at PA 95°. LASCO background subtracted and wavelet-processed images are shown in Figure 7. In UVCS the ray is observed in Lyα and O VI at several heights but not in Si XII . In the middle panel of Figure 7 the O VI intensities show very clearly the ray at 2.74, 2.29 and 1.95 $R_\odot$. The UV lines overlap very well with the WL ray as is also shown in the normalized intensities of Figure 8. In this figure the WL intensities were extracted along the white dashed line of Figure 7 at a height of 2.4 $R_\odot$ and compared in the middle panel with the UV O VI 1032Å intensities at three heights.

From the 60 of the 157 WL-selected rays which were also detected in UV spectra, only 10 were observed in the [Fe XVIII] line. Of the remaining rays, 34 did not have the necessary wavelength range to observe the [Fe XVIII] line, and in 16 the [Fe XVIII] line was within the wavelength band but not observable due to blending with the bright Lyα line in the redundant path. For further analysis, we have reorganized the 60 WL selected rays and the 18 UVCS selected features into a set of events that show [Fe XVIII] (Table 1) and a set that do not (Table 2). The [Fe XVIII] provides a strong constraint on the plasma temperature, and events where it is measured merit more detailed analysis than the events that do not.

A common characteristic of the UV rays is that hot and coronal lines are often offset. An example is shown in Figure 9. The figure shows the ray observed on 2003 November 4 after the CME at 19:54

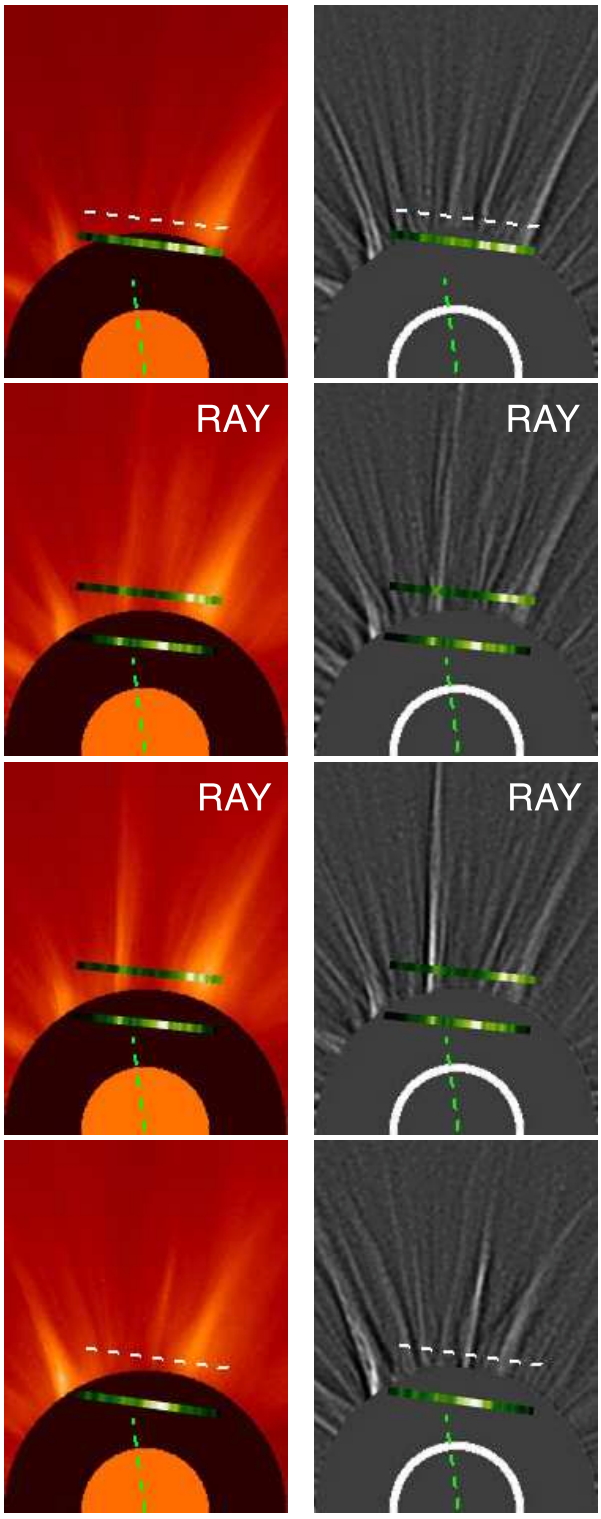

FIG. 5.— LASCO C2 images and wavelet-processed of the ray associated to the CME on 2001 May 12 at 23:00 UT with superimposed the Si XII 499Å intensity image along the UVCS slit. From the top the sequence shows the pre-CME corona on 2001 May 12 at 22:15 with Si XII image from 21:34 to 22:25 UT at 1.97$R_\odot$, two images of the ray on 2001 May 13 at 02:41 and 05:50 UT in LASCO C2 and Si XII at 2.42$R_\odot$, from 03:48 to 05:31 UT. The bottom images show the post-ray corona in LASCO C2 at 19:30 UT and UVCS Si XII, at 1.67$R_\odot$, from 19:28 to 20:17 UT. The white dashed line marks the position at which the LASCO data have been extracted when the UVCS slit was located below the occulter disk.

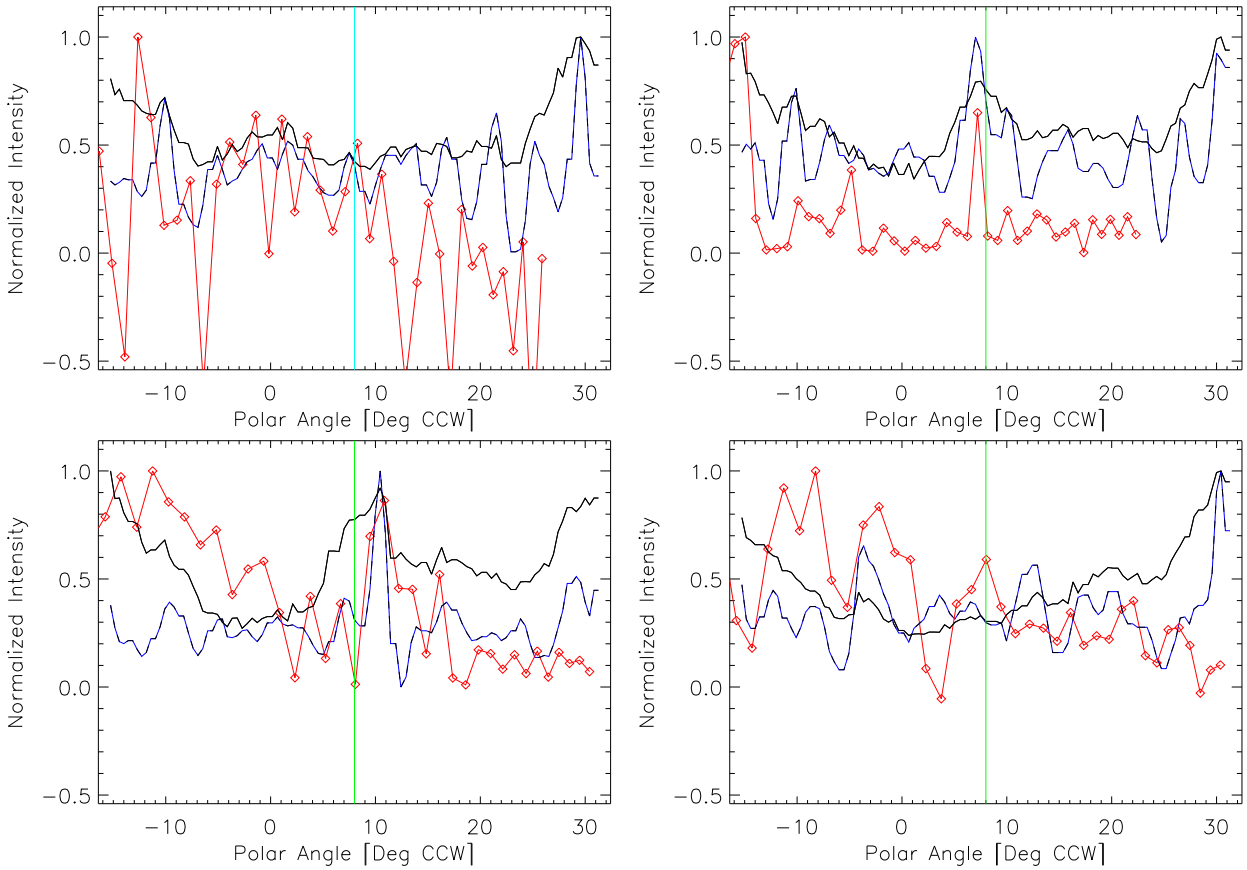

FIG. 6.— Sequence of normalized intensity cuts at 2.42$R_\odot$, of C2 LASCO background subtracted images (black) and wavelet-processed images (blue), with superimposed the normalized Si XII 499 Å intensity observed along the UVCS slit (red). The top left panel shows the pre-CME LASCO C2 on 2001 May 12 at 22:15 and UVCS Si XII 499 Å at 1.97$R_\odot$ from 21:34 to 22:25 UT. The top right panel shows the WL ray on 05/13 at 02:41 UT and UVCS Si XII 499 Å at 2.42$R_\odot$ from 03:48 to 05:31UT. The bottom left panel shows the WL ray on 2001 May 13 at 05:50 UT and UVCS Si XII 499 Å at 1.67$R_\odot$ from 05:33 to 06:05 UT. Finally the bottom right panel shows the post-ray WL corona on 2001 May 13 at 19:30 UT and UVCS Si XII 499 Å at 1.63$R_\odot$ from 19:28 to 20:17 UT. The intensities are the same as in Figure 5. Green line marks the polar angle of the WL ray.

UT (Ciaravella and Raymond 2008). The comparison among the lines of [Fe XVIII] (left panel), Si XII Ł521 (middle panel) and O VI Ł1032 (right panel) shows the displacement between coronal and hot lines. While characteristics of the rays such as line intensities and widths, are quite simple to compute in those lines not usually present in the solar corona, e.g. [Fe XVIII] and [Ca XIV] , the separation of the ray peak from the surrounding background corona is sometimes ambiguous for typical coronal lines, e.g. Si XII , O VI , Lyα , etc. For that reason we report the line intensities and widths for the rays observed in [Fe XVIII] , and in those cases we also report the intensities for the cooler lines. We select the same spatial regions for all the lines, subtracting a background based on the intensity distribution along the slit. The widths were computed as FWHM of the spatial distribution of the [Fe XVIII] line.

4.1. *Hot Rays*

The 28 rays with [Fe XVIII] emission are listed in Table 1. Only 10 of the rays selected from the white light ray catalog show [Fe XVIII] emission. The remaining 18 candidates come from the UVCS CME catalog and 15 of them are outside the time periods selected for the LASCO study. It is important to note that the PA of the WL and UV rays in Table 1 are different for several reasons. First, the PAs of WL rays are measured above the occulter disk (i.e. $\geq$ 2.5 $R_\odot$) at the time of first detection, while UV rays are mostly observed below the occulter, often later that the WL rays. Moreover, the rays are often not radial and move during their lifetime. The temperatures listed in Table 1 were computed using the ratio between [Fe XVIII] and Si XII lines under the assumption of ionization equilibrium. For the events in which only [Fe XVIII] was observed the temperature is not easily constrained. We used 'hot' to indicate that the temperature in the ray is higher than in the case in which Si XII was also present.

In twelve cases the narrow [Fe XVIII] emission has either no associated WL ray or a ray which did not satisfy the current sheet selection criteria. For those events no delay time is listed. For the remaining rays the delay time varies from cases in which the rays were detected earlier than in WL (negative numbers) to the most extreme UV observation where the ray was detected 21 hours later. In some cases the ray has been observed at several heights. All the heights at which [Fe XVIII] has been detected are below the LASCO C2 occulter disk, with the highest at 1.9 $R_\odot$.

Figure 10 shows the [Fe XVIII] line intensities as a function of the heliocentric distance for all the rays listed

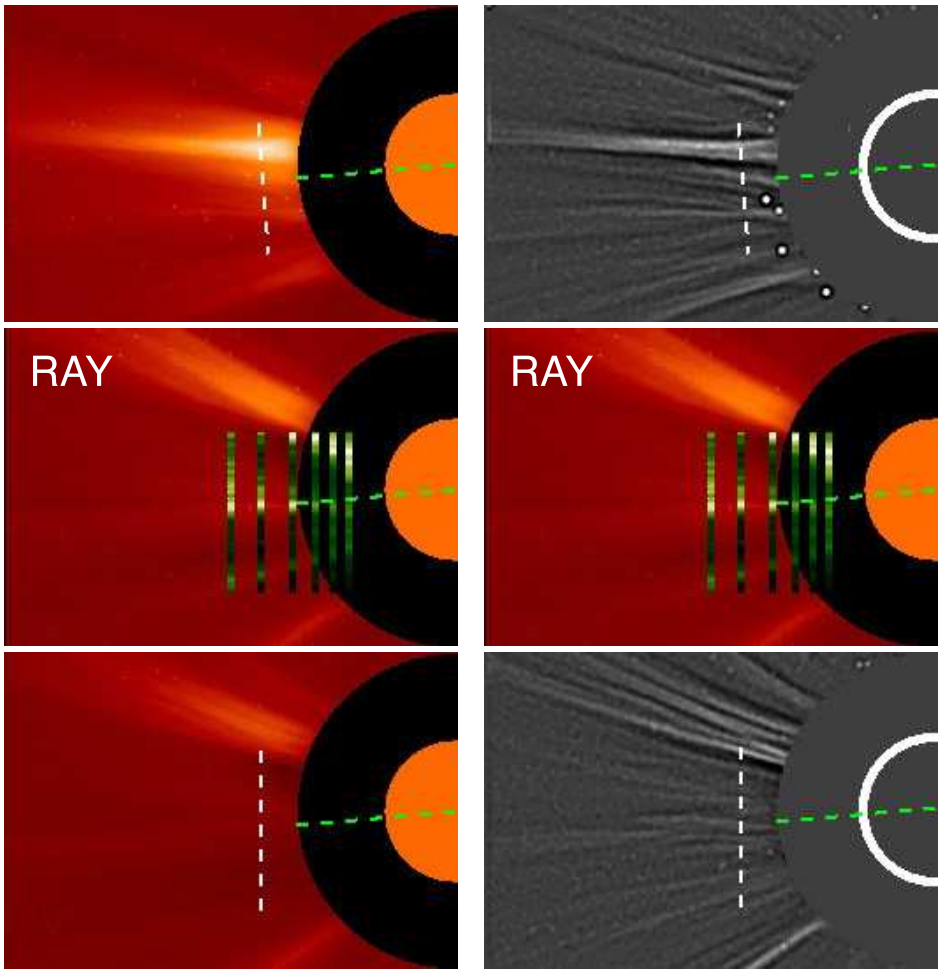

FIG. 7.— LASCO C2 images and wavelet-processed of the ray associated to the CME on 1998 April 23 at 05:27 UT. The top panels show the pre-CME corona on 1998 April 23 at 03:55 UT. The middle panel show the ray at 15:27 UT with superimposed the O VI 1032Å intensity image at several heights along the UVCS slit. The bottom panel the post-ray corona at 22:27 UT. The green dashed line marks the position of the white light ray, while the white dashed line mark the position along which LASCO data have been extracted for Figure 8.

in Table 1. In the top panel crosses, stars, diamonds and triangles correspond to different ranges of delay time. The squares are [Fe XVIII] bright narrow features with no corresponding rays in WL images. For those cases it was not possible to evaluate the delay time. The [Fe XVIII] line intensity ranges over three orders of magnitude or, (0.3 - 190) $\times$ 10^8 ph $cm^{-2}s^{-1}$. In the bottom panel the rays associated with halos, partial halos and narrow CMEs are plotted using diamonds, dots and triangles, respectively. The [Fe XVIII] line intensity in the ray decreases with the height but it does not show correlation with the delay time of the observation. Rays associated with energetic events such as halo and partial halo CMEs do not show the highest intensities in [Fe XVIII] line. The four rays associated with halos have intensities above 10^9 ph $cm^{-2}s^{-1}$ but the partial halos are scattered over the entire range of the observed intensities. In halo and partial halo events, the ray might be far from the plane of the sky, so that the actual position observed is greater than the apparent height. This likely accounts for the lack of correlation.

The [Fe XVIII] line intensity as function of the associated CME speed is plotted in Figure 11. One might expect that CME speed is related to Alfvén speed and that the magnetic energy available to heat the plasma is roughly proportional to V_A^2. In the top and bottom panels of the figure the CME linear and second order speed from LASCO catalog are used. Rays associated with narrow, halo and partial halo events are plotted with triangles, diamonds and dots respectively. The vertical dotted line indicates the LASCO average speed (445 km s^{-1}) for normal CMEs during the period 1999-2007 (Mittal et al. 2009). More than 78% of the hot rays are associated with CMEs with speed higher than the average LASCO speed. Again no strong correlation is seen in these plots although rays associated with partial halos and halos show some correlation with the speed of the CMEs. Above 1200 km s^{-1} [Fe XVIII] line intensities increase with the CME speed.

One might expect that the densities within a CME would be larger in more massive events, and that the correspondingly higher emission measures would yield higher intensities. No mass and energy estimates are available in the LASCO catalog for partial halo, halo and narrow CMEs. For all the other rays no strong correlation between [Fe XVIII] line intensity and energy of the associated CME has been observed. It is possible that this lack of strong correlation results from the vari-

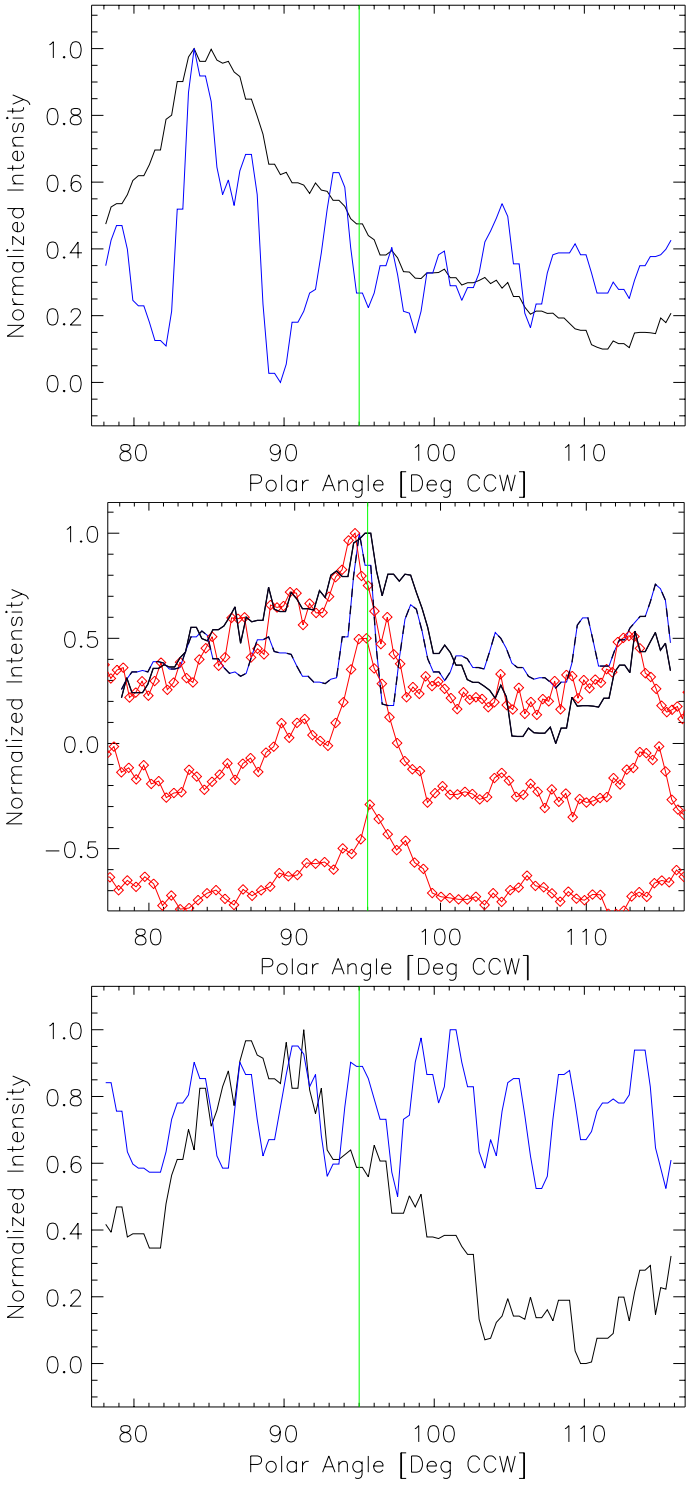

FIG. 8.— Sequence of normalized intensity cuts at 2.47$R_\odot$, of C2 LASCO background subtracted images (black) and wavelet-processed images (blue). Green line marks the polar angle of the WL ray. Upper panel shows LASCO C2 pre-CME on 1998 April 23 03:55 UT, middle panel shows LASCO C2 ray on 1998 April 23 15:27 UT and O VI 1032Å at 3 different heights: 2.74$R_\odot$ (upper red line) on 1998 April 23 from 14:46 to 15:04 UT, 2.29$R_\odot$ (middle red line) on 1998 April 23 from 14:27 to 14:45 UT, and 1.95$R_\odot$ (lower red line) on 1998 April 23 from 14:13 to 14:26 UT. The O VI line intensities have been offset in order to show them in the same plot. Lower panel shows LASCO C2 post ray on 1998 April 23 22:27 UT. The intensities are the same as in Figure 7.

ation of temperature among the different events, since the [Fe XVIII] intensity depends on both emission measure and temperature.

The spatial widths of the CS in Table 1 vary in the range (3 - 35) $\times$ 10^9 cm. While these widths are far larger than the widths expected for resistive reconnection in the corona, they are in reasonable agreement with predictions of turbulent reconnection (Lazarian & Vishniac 1999) or with the exhaust region of Petschek reconnection half a solar radius from the diffusion region, especially if the current sheet is not viewed edge-on. The widths of the [Fe XVIII] features are generally much smaller than the widths of associated features seen in Si XII, O VI or Lyα. We found no dependence of the width on the heliocentric height, the observation delay, or CME speed.

The ray temperatures range between ($\sim$ 3 - 8) $\times$ 10^6 K. The ten events in which the ray has been observed in the [Fe XVIII] line only, indicated with 'hot' in Table 1, are not associated with particularly energetic events. The estimated temperature range is the range where the [Fe XVIII] ionization fraction is large enough that the line is observable. Evidence for higher current sheet temperatures is found in the observations of [Fe XXI] and Fe XXIV (Innes et al. 2003) and Fe XXIII (Reeves & Golub 2011; Cheng et al. 2011). Recent Hinode/Extreme Ultraviolet Imaging Spectrometer observations of an event that shows Fe XV but no higher ionization states provide evidence for a current sheet cooler than 3×10^6 K (Landi et al. 2012).

4.2. *Spatial Offsets*

Half of the rays listed in Table 2 show a clear offset between the spatial positions of the peaks on [Fe XVIII] and Si XII. Figure 9 is a good example, in which the [Fe XVIII] peaks on the northern edge of the ray, Si XII is a broad feature centered on the ray, and O VI peaks on the southern edge of the ray. The current sheet studied by Ko et al. (2003) is another good example (see Figure 12 of that paper). In a few cases, Si XII or O VI show two peaks, with the [Fe XVIII] peak lying between them. In the cases where there is no offset, the [Fe XVIII] peak is usually narrow, while the Si XII peak is broader and the O VI peak is still broader.

One possible interpretation of the offset is that the cooler material is ambient coronal plasma about to be swept into the current sheet. The transverse motions seen in the Extreme-ultraviolet Imaging Telescope images by Yokoyama et al. (2001), Lyα emission observed with UVCS by Lin et al. (2005) or AIA images by Takasao et al. (2012) show inflow speeds of the order of 5 to 100 km s^{-1}. At those speeds, the coronal material would be swept into the current sheet on timescales of order 1-10 hours. Since the coronal gas is generally located to one side of the hot material, the inflow into the current sheet would be very asymmetric, a situation simulated by Murphy et al. (2012). This can lead to transverse motion of the current sheet, as reported by Ko et al. (2003).

An alternate interpretation of the offsets is that the cool material is essentially separate from the current sheet, occupying nearby field lines in a streamer-like structure, in which the inflow time to the current sheet

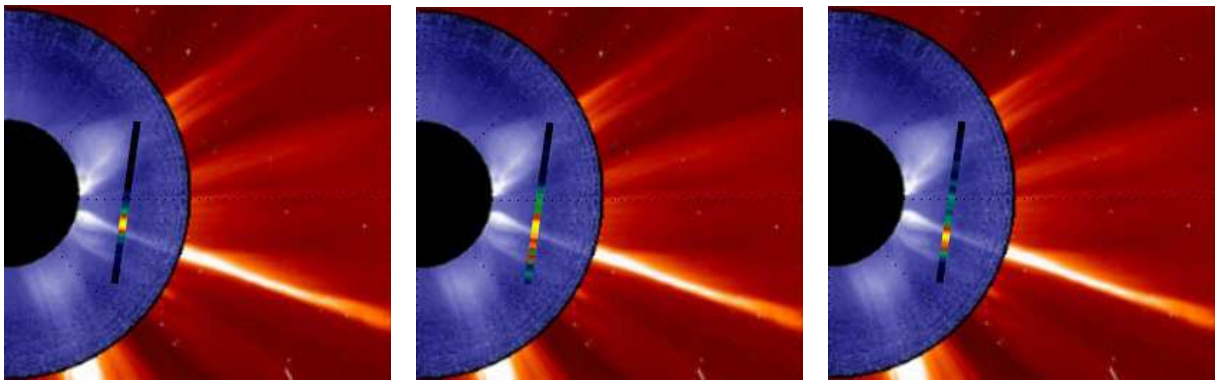

FIG. 9.— Composite image of the ray detected on 2003 November 4 by LASCO C2 at 23:54 UT, MK IV at 23:57 and UVCS from 20:12 to 20:51 UT. The three panels show UVCS images of [Fe XVIII] (left panel), Si XII (middle panel) and O VI lines (right panel).

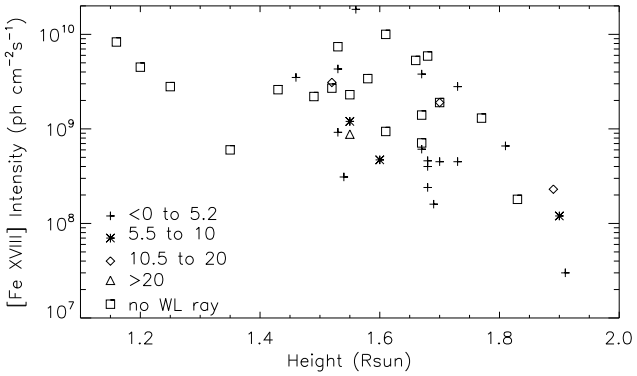

FIG. 10.— [Fe XVIII] line intensities as function of the heliocentric distance. The symbols refer to different delay time in hour (top panel), and CME morphology (bottom panel). In the bottom 4 CMEs are halos, 7 partial halo and 2 narrows with width of 14 and 44°.

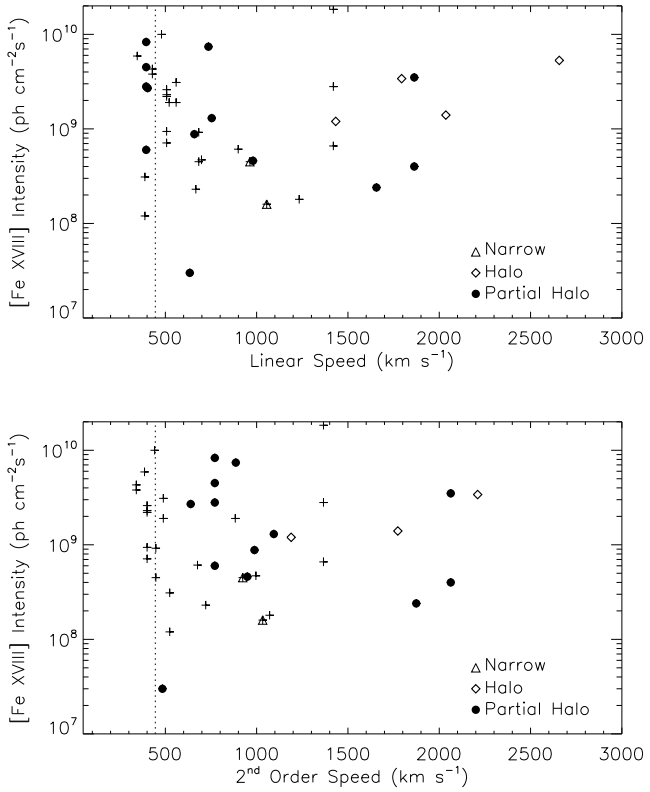

FIG. 11.— [Fe XVIII] line intensities as function of the CME linear (top panel) and second order speed (bottom panel). Triangles, diamonds and dots indicate the rays associated to narrow, halo and partial halo CMEs respectively. The vertical dotted line marks the average speed of CMEs during 1996-2007 period.

is longer than the flow time along the magnetic channel. This interpretation is suggested by the cool blobs that move beside the hot current sheet in the 2003 November 4 event (Ciaravella and Raymond 2008).

In general it is difficult to discriminate between the two interpretations above, but detailed study of individual events should make it possible to distinguish between them in some cases.

4.3. *Projection Effects*

Since we are observing optically thin structures, it is difficult to tell whether the apparent width we observe is the actual thickness of the current sheet or the result of thin sheet of gas viewed at an angle. In a few cases the projection effects can be shown to be small, as in the observation of a gap (i.e., a region of very low line intensity), rather than a bright region, in Lyα (Lin et al. 2005) and the case in which the column density in white light and the emission measure from UVCS can be combined to separate the density and thickness of the structure (Ciaravella and Raymond 2008). The offsets discussed in the previous section show that projection effects cannot be too large in those events, as the [Fe XVIII] and the other lines would be superposed if the angle to the line of sight was substantial.

4.4. *Coronal Rays*

Table 2 presents a list of events where [Fe XVIII] emission was not observable due to the UVCS instrument configuration (indicated by -) or observable but not detected (indicated by x). We also indicate whether the ray was detected (indicated by +) or not in the Si XII , O VI and Lyα lines. Of the 50 events in Table 2, 35 show both Si XII and O VI lines, so their temperatures are at least as high as that of the ambient corona. One shows Si XII without O VI or Lyα , indicating a temperature substantially higher than the ambient corona. However, as mentioned above there are often offsets between the features seen in different lines, so in some cases there may be a high temperature adjacent to a cooler one. For example, the 2003 November 4 event shown in Figure 9 has a bright ray in [Fe XVIII] and Si XII , but O VI and C III emission are offset several degrees to the north.

No correlation has been observed between the rays with coronal temperatures and the speed or energy of the associated CMEs. The range of linear speed of those rays varies between 100 and 1500 km s^{-1} . In particular the ray with the highest temperature, 'hot' in Table 2, is associated with a CME of speed $\sim$ 100 km s^{-1} .

4.5. *Cool Rays*

Table 2 also lists 14 events that were detected in O VI and/or Lyα , but not in Si XII or [Fe XVIII] . The ranges of delay time and height of UVCS observations are similar to those of the coronal or hot rays. These features are cooler than the ambient corona. In some cases, lines of C III or O V were detected, indicating much lower temperatures, on the order of 10^5 K. In some of those events, the line width of the Lyα line was clearly much smaller than the width of the coronal Lyα line, indicating proton temperatures of 10^5 K or less. Bright, long-lasting ray-like features in cool emission lines in the wakes of CMEs are not uncommon in UVCS spectra, but in most cases they do not satisfy the criteria for current sheets in LASCO. They are rather surprising, in that they often last for many hours, which is much longer than the free-fall time from heights of 1.5 to 2 R$_\odot$. These features may be prominence plasma from the CME core slowly draining back along particular magnetic field lines from much larger heights. Downflow of hot and cold material in the wake of a CME associated to an erupting prominence has been reported by Tripathi et al. (2007). As for the coronal rays, the cool rays are associated with CMEs with a wide range of speed and energy, including one halo and two partial halos.

4.6. *No UV Ray*

Many of the WL selected rays, 97 out of 157, did not show any corresponding UVCS features, mostly because UVCS was observing a different region during the WL ray lifetime. We do not include them in this study, but they will be considered in a paper on the white light rays alone (Webb 2012, in preparation). In a few cases, there may be no identifiable UV feature because the temperature was so high that it lay outside the 10^4 to 10^7 K range covered by the UVCS lines. In that case, it might show up as a gap in all the lines, as in the event discussed by Lin et al. (2005). It might also appear in hard X-ray observations as in the event reported by Sui & Holman (2003). More commonly, however, the UVCS data were not taken at the right position during the duration of the WL ray. In other cases UVCS data were too noisy due to short exposure time or confusion with other CME features, or the height of observation was too large.

5. SUMMARY AND CONCLUSIONS

A sample of 157 WL rays observed by LASCO, with an outward moving U or V-shaped structure detected in the wake of CMEs, has been used to search archival UVCS data in order to study their UV spectra. The sample included rays selected during both solar minimum (July 1996 - December 1998) and solar maximum (year 2001). In 60% of the WL sample, no UV rays were seen. Aside from the cases in which the UVCS instrument was observing a different target during the lifetime of the WL rays, a temperature higher than 10^7 K or a modest plasma emission measure would make the ray too faint for UVCS to detect. Sixty rays (40%) of the WL sample showed UV emission. Of those 60 WL rays, 14, or 23%, showed only cool gas, probably from prominence material draining back from the CME core. Of the 26 events for which [Fe XVIII] could be detected if present, 10 of them, or 38%, did show [Fe XVIII]. Many of the others had ordinary coronal temperatures, but a few showed strong enough Si XII emission to indicate relatively hot gas. Other rays may have been too hot to show [Fe XVIII] (T$>$ 10^7 K). We conclude that about 23% of the rays selected from LASCO images are magnetic flux tubes containing cold material, about 18% are hot features consistent with the current sheet interpretation, and the remaining 59% with ordinary coronal temperatures may be more quiescent streamers that have reformed after the eruption.

We also considered a sample of 18 more rays detected in the [Fe XVIII] line by UVCS. Most of them were outside the periods selected from the LASCO study. Ten out of 18 UV selected rays had no associated WL ray. While it is difficult to quantify the sensitivity of the white light search, since in many cases it is determined by the complex background of the evolving post-CME structure, it may be that the cases with no white light ray are examples of localized hot features with relatively small density enhancements or thicknesses.

Thus, WL images and UV spectra were analyzed for a total of 78 rays. The CME characteristics of the sample are quite broad in terms of speed, angular width and energy. Eight halo and 12 partial halo CMEs are in the sample. 70% of the rays were associated with CMEs with linear speed higher than the average speed of 445 km s^{-1} obtained by Mittal et al. 2009 for 1996-2007 period. This is expected as about 64% of the rays were detected during 2000-2003, the long lasting solar maximum of Cycle 23, and more than 50% of the 28 rays detected during solar minimum have speed higher than 445 km s^{-1} .

The 78 rays were divided in two sub-samples with (see Table 1) and without (see Table 2) [Fe XVIII] emission. The high temperature line [Fe XVIII] is not usually present in the solar corona and the rays observed appear more distinct from the background in this line than in typical coronal lines such as Si XII , O VI and Lyα , providing a simpler estimate of the line intensity and width of the rays, and strong constraints on their

plasma temperature. Based on the lines detected in the UV spectra the temperature of the rays were estimated. 37% of the rays had high temperature as indicated by the presence of [Fe XVIII] emission, 45% had temperature similar to the surrounding corona as indicated by the presence of Si XII , O VI and HI Lyα lines, and 18% were cool rays detectable only in O VI and/or HI Lyα lines with temperatures around 10^5 K. Of the WL rays without [Fe XVIII] , only in 14 cases was the line in the observed wavelength range and not detected. In all the other cases especially in those that had Si XII we cannot exclude that [Fe XVIII] could have been present as well.

Rays with [Fe XVIII] emission are mostly (85%) associated with CMEs occurring during solar maximum. In the sample of rays with no [Fe XVIII] only 52% are during solar maximum. Although the range of CME speed associated with the rays is very wide in both samples, the average and median speeds of the rays that show [Fe XVIII] are higher than those that do not. All the rays showing [Fe XVIII] emission have been observed at heights below the LASCO occulter disk.

The temperatures of the rays detected in [Fe XVIII] line are higher than $10^{6.5}$ K, but this is essentially a selection effect due to the formation temperature of [Fe XVIII] . No dependence on the height has been observed. The spatial widths range between 3 and 35 $\times$ 10^9 cm and again no correlation with the speed, delay and height exists. The WL widths of four of the hot rays have also been estimated by Song et al. (2012) at 3 and 4 $R_\odot$, and they are in agreement with those obtained from the [Fe XVIII] emission. There is a trend of [Fe XVIII] intensity to decrease with the height. This is also observed in the few cases in which the same ray was observed at different heights.

A wide range of [Fe XVIII] line intensities has been detected, but no strong correlation has been observed with the delay time of the UV observations, or morphology of the associated CMEs. The intensity of the [Fe XVIII] line in the ray associated with the 2002 January 8 CME (Ko et al. 2003), measured with about 50 h delay, is among the highest. The four rays associated with halo CMEs have [Fe XVIII] intensities well within the range of intensities detected for the CS associated to other CMEs.

No significant correlation of the [Fe XVIII] intensity has been observed with CME speed or energy except for the halo and partial halo events. Above 1200 km s^{-1} there is a weak trend of [Fe XVIII] intensity to increase with the speed.

The results outlined above provide a wide range of UV properties of WL rays, but no strong correlations with the associated CME speed, energy and morphology has been found. While the hot and coronal rays may fit within the framework of the reconnection processes that bring ambient plasma into CS structures, the much lower temperatures observed in the cold rays suggest a different interpretation. These may be channels of cold prominence material draining back from the CME core as it moves outwards through the solar corona.

This work was performed under NASA grants NNX09AB17G-R and NNX11AB61G to the Smithsonian Astrophysical Observatory. It was initiated during a series of workshops on *Understanding the role of current sheets in solar eruptive phenomena* at the International Space Sciences Institute (ISSI). We also benefited from the SOHO/LASCO CME catalog, generated and maintained by the Center for Solar Physics and Space Weather, The Catholic University of America in cooperation with NRL and NASA.

REFERENCES

Bemporad, A., Poletto, G., Suess, S. T., Ko, Y.-K., Schwadron, N. A., Elliott, H. A., Raymond, J. C. 2006, ApJ, 638, 1110
Brueckner, G.E., et al. 1995, Sol. Phys., 162, 357
Cheng, X., Zhang, J., Lium Y., & Ding, M.D. 2011, ApJ, 732, 25
Caravella, A., Raymond, J. C., Li, J., Reiser, P., Gardner, L. D., Ko, Y.-K., Fineschi, S. 2002, ApJ, 575, 1116
Ciaravella, A., and Raymond, J. C. 2008, ApJ, 686, 1372
Emslie, A. G., Miller, J. A., and Brown, J. C. 2004, ApJ, 602, L69
Forbes, T. G., et al. 2006, Space Sci. Rev., 123, 251
Forbes, T. G. 2000, J. Geophys. Res., 105, 23153
Gardner, L.D., et al. 2002, in "The Radiometric Calibration of SOHO",ESA SR-002, edited by A. Pauluhn, M.C.E. Huber and R. von Steiger, p.161
Giordano, S., Ciaravella, A., Raymond, J. C., Ko, Y.-K., and Suleiman, R. 2013, J. Geophys. Res., in press
Howard, T.A., DeForest, C.E. & Reinard, A.A. 2012, ApJ, 754, 102
Innes, D.E., McKenzie, D.E., & Wang, T. 2003, Sol. Phys., 217, 247
Ji, H., & Daughton, W. 2011, Phys. Plasmas, 11, 111207
Ko, Y.-K., Raymond, J. C., Lin, J., Lawrence, G., Li, J., Fludra, A. 2003, ApJ, 594, 1068
Kohl, J.L., et al. 1995, Sol. Phys., 162, 313
Landi, E., Raymond, J.C., Miralles, M.P., & Hara, H. 2012, ApJ, 751, 21
Lazarian, A., & Vishniac, E.T. 1999, ApJ, 517, 700
Lin, J., & Forbes, T. G. 2000, J. Geophys. Res., 105, 2375
Lin, J., Ko, Y.-K., Sui, L., Raymond, J. C., Stenborg, G. A., Jiang, Y., Zhao, S., Mancuso, S. 2005, ApJ, 622, 1251
Litvinenko, Y. E. 1996, ApJ, 462, 997
Loureiro, N.T., Schekochihin, A.A., & Cowley, S.C. 2007, Phys. Plasmas 14, 100703
Low, B. C. 2001, J. Geophys. Res., 106, 25141
Mittal, N., Pandey, K., Narain, U., Sharma, S.S. 2009, Ap&SS, 323, 135
Murphy, N.A., et al. 2012, ApJ, 751, 56
Patsourakos, S., Vourlidas, A. 2011, A&A, 525, 27
Priest E., Forbes T. 2000, in Magnetic Reconnection, Cambridge Univ. Press
Raymond, J.C., Ciaravella, A., Dobrzycka, D., Strachan, L., Ko, Y.-K., Uzzo, M., Raouafi, Nour-Eddine 2003, ApJ, 597, 1106
Reeves, K.K., & Golub, L. 2011, ApJ, 727, L52
Savage, S.L., McKenzie, D.E., Reeves, K.K., Forbes, T.G., & Longcope, D.W. 2010, ApJ, 722, 329
Savage, S.L., & McKenzie, D.E. 2011, ApJ, 730, 98
Schettino, G., Poletto, G., Romoli, M. 2010, ApJ, 708, 1135
Song, H.Q., Kong, X.L., Chen, Y., Li, B., Li, G., Feng, S.W.,Xia, L.D. 2012, Sol. Phys., 276, 261
Stenborg, G., Cobelli, P. J. 2003, A&A, 398, 1185
Sui, L., & Holman, G.D. 2003, ApJ, 596, L251
Takasao, S., Asai, A., Isobe, H., & Shibata, K. 2012, ApJ, 745, 6
Tripathi, D., Solanki, S.K., Mason, H.E., Webb, D.F. 2007, A&A, 472, 633
Vršnak, B., et al. 2009, A&A, 499, 905
Wang, T., Sui, L., Qiu, J. 2007, ApJ, 661, L207
Webb, D. F., Cliver, E. W. 1995, J. Geophys. Res., 100, 5853
Webb, D. F., Burkepile, J., Forbes, T. G., Riley, P. 2003, J. Geophys. Res., 108, 1440
Yokoyama, T., Akita, K., Morimoto, T., Inoue, K., & Newmark, J. 2001, ApJ, 546, 69

TABLE 1
RAYS WITH [Fe XVIII] EMISSION

CME	LASCO Ray			MK4	Sel	Δt C2/ UVCS	UVCS			Lines 10^8 ph s^{-1}cm^{-2}sr^{-1}				Width 10^9 cm	Log T
	Time	PA	Durat.				Time	PA	$R_\odot$	Fe XVIII	Si XII	OVI	Lyα		
97-05-05 06:30[a]	-	-	-		W		05:16:38	71	1.35	6.	157	x	x	7	
							05:16:59	69	1.25	28	228	x	x	6	
							05:17:21	69	1.20	45	420	x	x	3	
							05:17:36	69	1.15	83	900	x	x	4	6.5
98-03-23 09:33[b]	-	-	-	N	U	-	23.16:00	257	1.52	27	78	x	x	12	6.7
98-04-20 10:07[c]	15:27	262-250	14	-	W	4.0	20.19:30	247	1.46	35	x	x	x		hot
						4.2	20.19:36	247	1.68	4.0	x	x	x	6	”
00-02-22 14:06	-	-	-		U		22.18:33	47	1.43	26	x	x	x	9	hot
							18:50	48	1.49	22	x	x	x	12	”
							19:01	45	1.55	23	x	x	x	18	”
							19:12	46	1.61	9.4	x	x	x	12	”
							19:23	45	1.67	7.1	x	x	x	12	”
00-09-23 21:26	01:27/24	300	21	Y?	U	-3.1	23.22:19	302	1.67	38	x	x	x	6	hot
						-3.0	22:29	302	1.53	43	x	x	x	8	”
01-01-26 16:06	21:08	52	?	Y?	W	7.0	27.04:06	52	1.60	4.7	120	71	5.2	6	6.50
01-07-05 05:54	07:54	127	9	-	W	3.2	05.11:07	125	3.12	x	x	0.5	5.5		
						3.5	11:25	126	2.58	x	x	1.9	4.6		
						4.0	11:52	126	2.13	x	x	1.7	24		
						4.5	12:23	124	1.73	4.5	x	39	-	15	
						4.7	12:33	130	1.55	x	10	130	720		
01-07-20 13:31	18:06	80	>9	Y?	W	15.4	21.09:27	84	3.11	x	x	0.95	350		
						15.6	21.09:44	84	2.56	x	x	3.2	110		
						16.1	21.10:12	83	2.12	x	x	15	420		
						16.4	21.10:29	81	1.89	2.3	380	12	5700	8	6.42
						16.6	21.10:42	83	1.70	x	10	51	1300		
						16.8	21.10:52	84	1.53	x	16	130	1900		
01-08-25 16:50	17:50	128	?	Y	W	6.7	26.00:29	125	1.55	12	45	x	x	17	6.65
01-09-21 08:54	11:30	117	33.6	Y	W	21.4	22.08:32	115	1.55	8.8	x	x	x	13	hot
01-10-05 21:08	21:30	260	21	Y	W	4.8	06.02:16	263	1.70	4.5	110	200	x	8	6.50
						5.0	02:29	261	1.53	9.2	390	480	x	6	6.52
01-10-30 18:16[h]	-	-	-	-	U	-	31.04:27	92	1.53	74	x	x	x	20	hot
01-11-01 03:30	09:54	272	∼38	Y?	W	16.3	02.02:11	273	1.70	19	61	57	300	8	6.63
						16.5	02:23	273	1.52	31	200	900	1000	6	6.58
01-12-20 21:12	00:54/21	282	>8	?	W	-1.6	20.23:20	280	1.54	3.1	x	x	-	15	hot
						8.4	21.09:20	278	1.90	1.2	1.6	x	-	13	6.72
01-12-29 09:54	12:30	280	3	-	U	-1.8	29.10:41	282	1.91	0.3	x	x	x	6	hot
02-01-08 17:54[d]	-	-	-	-	U	-	10.20:45	83	1.58	34	420	30	1700	7	6.55
02-11-26 17:06[e]	-	-	-	-	U	-	27.02:00	305	1.61	100	x	x	x	6	hot
03-01-03 11:30	-	-	-	N	U	-	03.11:35	299	1.70	19	6.1	x	x	4	6.9
03-06-02 00:30[f]	01:54	248	>5	?	U	4.2	02.06:08	248	1.68	2.4	<0.4	33	x	27	6.9
03-06-02 08:54[f]	10:06	260	2	Y?	U	0	02.10:06	258	1.68	4.6	11	x	x	9	6.7
03-06-13 16:30	-	-	-	N	U	-	13.17:23	280	1.68	59	190	x	x	8	6.65
03-10-24 02:54	05:54	100	11	N	U	1.6	24.04:29	104	1.69	1.6	x	x	-	18	hot
03-10-24 05:30	-	-	-		U		24.06:35	128	1.83	1.8	x	x	-	6	hot
03-11-01 23:06	03:54/2	250	5.5	Y?	U	-3.8	02.00:06	249	1.67	6.1	110	x	-	35	>6.65
03-11-02 09:30	†	†	†	Y?	U	?	02.17:01	240	1.67	14	120	x	-	7	>6.75
03-11-03 10:06	10:55	275-272	∼5.6	N	U	0.2	03.11:07	267	1.81	6.6	30	x	x	20	6.75
						2.4	13:18	271	1.73	28	26	x	x	20	
						2.6	13:31	271	1.56	184	128	x	x	20	
03-11-04 19:54[g]	-	-	-		U		04.20:30	253	1.66	53	17	x	x	11	6.90
04-07-28 03:30	-	-	-	N	U	-	28.03:47	280	1.77	13	20	x	x	15	6.70

Starting from the left, the table lists the CME onset time as given in the LASCO catalog, the time at which the ray was first seen, the PA and the duration of the WL ray selected in LASCO, the MLSO/Mk4 data, and the observation used for selecting the ray, U for UVCS and W for WL. For the Mark4 we used '-' when the data were not available, 'N' and 'Y' when the data were available and the ray was not observed or observed, respectively. A question mark indicates an uncertain detection or case where the ray was not clear. In the seventh column is the delay time, in hours, between the first observation in LASCO and in UVCS. The eighth, ninth and tenth columns show the time, PA and height at which the ray was observed by UVCS. From column 11 to 14 are listed the line intensities of [Fe XVIII] , Si XII , O VI and Lyα . In these columns '-' indicates that the line was not observable due to the instrument configuration while 'x' indicates that the line was observable but not detected. The spatial width of the [Fe XVIII] emission and the estimated temperature of the ray are in the last two columns.

[a] The UV ray is associated to the same CME as the ray selected from WL but it does not satisfies the selection criteria

[b] Ciaravella et al. 2002. Many bright rays are seen in WL but not obiously related to the UV ray.

[c] The ray changes position during the observation

[d] Ko et al. 2003

[e] Bemporad et al. 2006

[f] Schettino et al. 2010

[g] Ciaravella & Raymond 2008

[h] CDAW catalog incorrectly lists at 20:42:06

† many rays, not clear

TABLE 2
RAYS WITH NO [Fe XVIII] EMISSION

CME	LASCO Ray			MK4	Δt	UVCS		Lines				Log T
	Time	PA	Durat.		C2/UVCS	Time	$R_\odot$	Fe XVIII	Si XII	OVI	Lyα	
96-08-22 08:38	09:38	119	>15h	N	6.0	22.15:39	$\leq$2.02	-	x	+	+	cool
96-10-19 02:39	3:56/20	126	20h	Y	16.2	20.10:46	2.31- 1.45	-	+	+	+	coronal
97-02-23 02:55	06:30	78	?	-	0.7	23.07:11	1.45-2.3	-	+	+	+	"
97-04-22 22:57	10:50/23	70	2.5d	?	2.8	23.13:04	1.42-3.11	-	+	+	+	"
97-05-07 10:26	22:16	277	18h	-	9.7	08.02:29	1.4-3.1	-	+	+	x	"
97-07-22 08:57	11:02	250	1.5d?	-	4.9	22.13:50	1.5-2.3	-	+	+	+	"
97-07-25 21:01	22:00	268	1.5d	?	4.0	26.01:48	1.42-4.1	-	+	+	+	"
97-08-26 00:00	10:53/27	80	1d	?	18.1	28.08:57	1.46-3.15	-	+	+	+	"
97-08-28 16:41	08:0/29	96	1.8d	Y?	-0.2	29.07:46	1.46-3.15	x	+	+	+	"
97-09-13 11:33	18:19/14	90	>1d	-	14.1	15.08:25	1.5-3.1	-	+	+	+	"
97-09-19 01:29	15:04	275	>19h	-	4.9	20.00:25	1.45-3.15?	-	+	+	+	"
97-09-28 14:28	20:59	90	1d	Y?	12.9	29.09:56	1.5-3.15	-	+	+	+	"
97-10-12 06:26	08:28	255	13h	Y?	4.6	13.02:04	1.5-2.3	-	+	+	x	"
97-11-22 05:45	21:30	45	1d	Y?	1.5	23.03:31	1.5-2.3	-	+	+	+	"
97-12-02 16:43	12:27/3	80	18h	-	15.6	04.08:59	1.5-2.3	-	+	+	?	"
98-03-23 00:50	08:13	85	days	Y?	1.1	23.09:06	1.5-3.17	-	+	+	+	"
98-03-27 20:07	01:04/28	195	15h	-	10.8	28.11:55	1.5-2.07?	-	+	+	+	"
98-03-29 03:48	10:06	190	>5	-	2.0	29.12:07	1.5-2.64	-	+	+	+	"
98-03-31 06:12	08:20	174	>7h	-	4.4	31.12:46	1.5-2.5	-	+	+	x	"
98-04-21 19:03	23:27	280	1.7d	Y?	-1.2	21.22:13	1.4-3.73	x	+	+	+	"
98-04-23 05:27	10:55	95	7.5h	N	1.6	23.13:34	1.48-3.17	-	x	+	+	cool
98-05-21 05:27	11:02	293	17.5h	Y	15.5	22.02:35	1.5 -3.2	-	x	x	+	"
98-06-02 08:08	17:27	246	3h	-	0.1	02.17:30	2.3	-	x	+	x	"
98-06-13 02:27	11:27	268	23h	Y?	3.0	14.00:30	1.48-1.95	-	+	+	+	coronal
01-01-02 21:30	11:54/3	40	12h	-	16.7	04.04:47	3.6-1.52	x	+	+	+	"
01-01-25 15:30	03:06/26	180	9h	N	2.0	26.05:04	4.15-3.6	x	x	+	+	cool
01-01-31 18:06	10:54/02	55	>9h	?	5.5	02.16:22	1.70-1.55	-	+	+	+	coronal
01-02-19 19:50	23:00	270	20h	?	3.9	19.02:55	1.71-1.53	-	+	+	+	"
01-03-04 05:50	08:26	40	?	Y	6.4	04.14:49	1.70-1.53	-	x	+	+	cool
01-03-18 02:26	06:06	108	9h	N	10.6	18.16:45	1.7-1.5	-	x	+	+	"
01-03-26 00:26	13:50	288	18.5h	N	2.4	26.16:12	1.7-3.1	-	+	+	+	coronal
01-04-22 05:26	13:06	160	?	?	-0.1	22.12:59	3.13-1.56	-	+	+	+	"
01-04-30 14:30	16:54	88	?	-	-0.1	30.16:50	1.7-1.5	-	+	+	+	"
01-05-12 23:00	02:21/14	8	$\sim$13.5h	-	-0.1	13.02:14	2.47-1.74	-	+	+	+	"
01-05-13/14 14:15	17:20	352	12h	-	2.0	13.19:17	1.63-2.42	-	+	+	+	"
01-05-31 03:08	07:31	247	24	-	12.2	01.05:44	1.70-1.53	x	x	+	+	cool
01-06-02 11:54	13:54	290	13h	?	2.6	02.16:33	3.1	x	x	x	+	"
01-07-19 10:30	11:06	230	14h	?	5.8	19.16:54	3.1-1.53	x	x	+	+	"
01-07-20 13:31	18:06	80	>9h	Y?	15.3	21.09:26	3.11-1.53	x	+	+	+	coronal
01-07-20 22:22	23:15	110	>12h	-	10.2	21.09:26	3.11-1.53	x	+	+	+	"
01-08-09 21:30	02:06/10	106	?	?	9.2	10.11:20	3.1-1.5	x	x	+	+	cool
01-08-21 12:06	2:27/22	234	>21h	Y?	5.4	22.07:51	1.7-1.5	x	x	+	+	"
01-10-01 05:30	07:31	200	24h	?	7.2	01.14:46	3.1-1.53	x	+	+	+	coronal
01-10-01 22:06	15:30/2	40	48h	Y	12.9	03.04:24	1.7-1.5	x	x	+	+	cool
01-10-13 05:54	18:39	130	3d	?	23.3	14.15:59	1.7-1.5	x	+	+	+	coronal
01-10-16 09:50	16:06/17	323	1d	-	18.9	18.10:59	2.1-1.5	x	+	x	x	hot
01-11-12 10:06	23:06	300	12h	-	3.9	13.03:00	3.1-1.5	x	+	+	+	coronal
01-12-12 18:30	23:54	113	24h	-	2.5	13.02:26	1.5-1.7	-	x	+	+	cool
01-12-14 09:06	09:06	75	24h	-	2.1	14.12:02	3.1-1.5	-	+	+	+	coronal
01-12-28 11:30	12:54	30-40	7.5h	?	2.2	28.15:04	1.7-1.5	-	+	+	+	"